CrystEngComm

Accepted Manuscript

ROYAL SOCIETY OF CHEMISTRY

www.rsc.org/crystengcomm

Journal Name

RSCPublishing

PAPER

Controlled synthesis of CuS caved superstructures and their application to the catalysis of organic dye degradation in the absence of light

Qun Wei Shu,[a,c] Jing Lan,[b] Ming Xuan Gao,[a] Jian Wang,[b] Cheng Zhi Huang*[a,b]

Cite this:

Received ooth January 2012,
Accepted ooth January 2012

DOI: 10.1039/xoxxooooox

www.rsc.org/

3-D CuS materials have attracted attention due to their unique catalytic properties. These materials are generally synthesized by the template method, however this process is time-consuming, complex, and results in low catalytic activity. In this paper, we describe a new method for the synthesis of monodispersed and highly-homogeneous CuS caved superstructures with a variety of shapes and sizes. Our synthesis was accomplished in 2.5h by a simple direct solvothermal reaction of $CuSO_4$ with sulfur powder under normal pressure, and accomplished using the reduction of acetaldehyde produced by ethylene glycol (EG) during the heating process. We show that the size and morphology of CuS products can be tuned by adjusting the molar ratios of reactants, reaction temperature and preheating temperature. The CuS caved superstructures prepared were highly catalytic, as shown by examining the degradation of methylene blue (MB) in the absence of light through the oxidation of hydroxide radicals produced by H_2O_2 in the catalytic reaction. This shows that CuS catalyst prepared by our novel method has efficient catalytic activity making it a cost-effective and convenient method for the treatment of dye-contaminated waste water.

1. Introduction

Metal chalcogenide clusters are interesting due to their unique, optical, photovoltaic and catalytical properties etc.[1-4] Especially, copper sulfide (CuS), a member of the transition metal chalcogenides, which is an important family of p-type semiconductors with superior optical, electrical, and other physical and chemical properties, has been extensively studied for its applications in the areas of lithium batteries and solar cells,[5-9] sensing,[10-16] photothermal therapy,[17-20] imaging,[21, 22] supercapacitance,[23, 24] drug delivery,[25] cathode materials,[26] nonlinear optical materials,[27] and catalysis.[28-35]

Among different types of CuS materials, those with 3-D structures have recently been researched as catalysts. This interest can be attributed to the large surface area, high surface-to-volume ratio, and sufficient surface active sites of CuS materials. This allows better contact between the reactants and the surface of CuS resulting in enhanced catalytic efficiency. In this application, 3-D CuS materials have been studied as a photocatalyst in dye degradation because they are nontoxic, inexpensive, and stable under ambient conditions,[28, 29, 31, 32, 34] enabling their use in the area of clean technology.

The applications of CuS materials are dependent on their properties, which are affected by their morphology, spatial orientation and structural arrangement. Currently, 3-D CuS in the shape of hollow spheres,[31, 36-43] hollow cages,[44-46] nano/microflowers,[32, 47-49] nano/microspheres,[33, 50] and hierarchical architectures[30] have been successfully synthesized by hydrothermal and solvothermal methods. However, these 3-D CuS structures were created using the aids of 3-D copper foam, Cu_2O particles by solution chemistry routes in atmospheric flasks or Teflon-lined autoclaves. The use of 3D copper foam is time-consuming and expensive and the use of a Teflon-lined autoclave is also time-consuming and involves operating under high pressure. The use of Cu_2O particles requires multiple steps, which is time-consuming and complex. In these template-based techniques complete removal of template material is difficult, which affects the purity of the final product. There are only a few reports on the synthesis of 3-D CuS materials without using a template or a Teflon-lined autoclave.[24, 51] Thus, the fabrication of 3-D CuS materials with high catalytic activity at atmospheric pressure through a simple, safe, template-free solvothermal process still remains a great challenge

In this study, a very simple, template-free solvothermal method was developed to synthesize 3-D CuS caved superstructures with homogeneous and monodispersed properties under normal pressure. The evolutionary diversification of the product morphology was also investigated based on the time-dependent scanning electron microscopy, and a possible growth pattern was proposed. Our synthesized CuS caved superstructures have high catalytic activity and could be directly applied to the treatment of dye contaminated waste water without the use of light, an improvement over methods reported in literature.[28-32, 34]

2. Experimental section

2.1 Materials

Sulfur powder, carbon disulfide (CS_2), 30% hydrogen peroxide (H_2O_2), ethanol (C_2H_5OH), ethylene glycol (EG) were purchased from Chengdu Kelong Chemical Co., Ltd., (Chengdu, China). Copper sulfate pentahydrate ($CuSO_4 \cdot 5H_2O$) was obtained from Tianjin Regent Chemical Co., Ltd., (Tianjin, China). Polyvinylpyrrolidone (PVP, *M*w=55000) and methylene blue (MB), were received in standard grade from Sigma-Aldrich Chemical Co., Ltd., (USA). All the reagents were of analytical grade and used without further purification. Double distilled water was used in all experiments.

2.2 Synthesis of 3-D CuS caved superstructures

In a typical synthesis, $CuSO_4$ (0.5 mmol) and PVP (0.075 g) were added to preheated EG (10 mL) solvent. The EG was preheated at 160 ^oC for 1 h, and the mixture was magnetically stirred to form a homogeneous blue-green solution at 160 ^oC. After 1.5 h, the blue-green solution was cooled to 120 ^oC. Simultaneously, sulphur powder (0.5 mmol) was added into the preheated EG (5 mL) at 120 ^oC for 40 min, and the solution became yellow in color with stirring. Finally, the yellow solution was added into the blue-green solution at 120 ^oC under normal pressure. After 10min, the grey-black precipitate was collected by centrifugation and washed with CS_2, ethanol and double distilled water several times. The synthetic method for the regular hexagonal CuS plates was the same as that of 3-D CuS caved superstructures, except that the temperature used for preheating the $CuSO_4$ was different.

2.3 Evaluation of catalytic activity

To assess the catalytic ability of 3-D CuS caved superstructures, methylene blue (MB), a typical dye resistant to biodegradation and direct photolysis, was employed. Typically, a sample of our dry 3-D CuS caved superstructures (0.01 g) was mixed with 10 mL of 3×10^{-5} M MB dye solution, and then kept in the dark under ultrasound for 10 min to ensure the establishment of an adsorption-desorption equilibrium. 300μL of 30 wt% H_2O_2 was added with slow agitation at 30 ^oC under both light and dark conditions. 700μL of the resultant mixtures were taken out at a given time interval and immediately centrifuged for the determination of MB concentration using a UV-vis spectrophotometer. The samples were centrifuged and the precipitation was collected and rinsed thoroughly with distilled water for further reuse.

2.4 Apparatus and characterization

The crystallographic structure of the fabricated products was analyzed using an x-ray diffractometer (XRD; Purkinje General instrument XD-3), while the morphology was measured with an S-4800 scanning electron microscope (FESEM, Hitachi, Japan) equipped with an energy-dispersive X-ray spectroscopy (EDS) system and a high resolution transmission electron microscope (HRTEM, FEI Company, USA). An X-ray photoelectron spectrometer (XPS, ESCALAB 250) was used to determine the composition of CuS caved superstructures. The Brunauer-Emmett-Teller specific surface area (SBET) of the powders was performed using a nitrogen adsorption apparatus (AS1-MP-9, Quantachrome, USA). Ultraviolet-visible (UV-Vis) spectra were recorded on a UV-vis spectrophotometer (UV3600, Shimadzu, Japan). Electron paramagnetic resonance (EPR) spectra were measured on a Bruker spectrometer (ESP-300E, Bruker, Germany) at room temperature.

3. Results and Discussion

3.1 Physical characterization.

The SEM images (Fig. 1a-c) of the prepared CuS show good dispersity, uniformity and regular morphology. Also the 3-D CuS caved superstructures were made up of several hexagonal or many triangular plates. There are some dark stripes and shady centers in the TEM image of CuS caved superstructures (Fig. 1d), indicating that 3-D particles were assembled by several hexagonal or many triangular plates. The lattice fringes (Fig. 1e) displayed with the 3-D CuS caved superstructures show well-defined crystal structures. The lattice spacing was 0.19 nm corresponding well to the (110) plane spacing of hexagonal CuS (JCPDS no.00-006-0464).

The purity, phase, crystallinity, and composition of our CuS products were determined by XRD, EDS and XPS (Fig 2). The XRD pattern from the CuS caved superstructures, shown in Fig. 2a, was compared with standard data for CuS. All the primary diffraction peaks of the CuS caved superstructures created under our solvothermal experimental conditions were consistent with the standard data obtained from hexagonal CuS(JCPDS no.00-006-0464), and the samples possess a single phase. The stronger peaks located at 29.28, 31.79, 32.82, 47.95 and 59.34 should be attributed to (102), (103), (006), (110) and (116) planes.[32] The presence of strong and sharp diffraction peaks also shows that our products are well crystallized, and the strongest peak along (110) indicates the preferential growth direction along the (110) plane of hexagonal CuS.[52]

The EDS spectrum (Fig. 2b) confirmed that the CuS caved superstructures consisted of copper and sulfur elements with a Cu:S ratio of 27:27, showing a 1:1 copper to sulfur ratio. Fig. 1c shows that the binding energies of Cu $2p_{3/2}$ and Cu $2p_{1/2}$ shift slightly left to 932.3 eV and 952.1 eV in the Cu2p region, and two shakeup lines corresponding to the satellite peaks of Cu^{2+} at 943.2 and 963.6 eV almost disappear. This indicates the presence of little Cu^{+} and mainly Cu^{2+}. Moreover, the XPS spectrum of S 2p (Fig. 2d) also reveals the binding energy of S $2p_{3/2}$ and S $2p_{1/2}$ peaks at 162.3 and163.4eV. These results indicate that our CuS caved superstructures are very pure.[53-57]

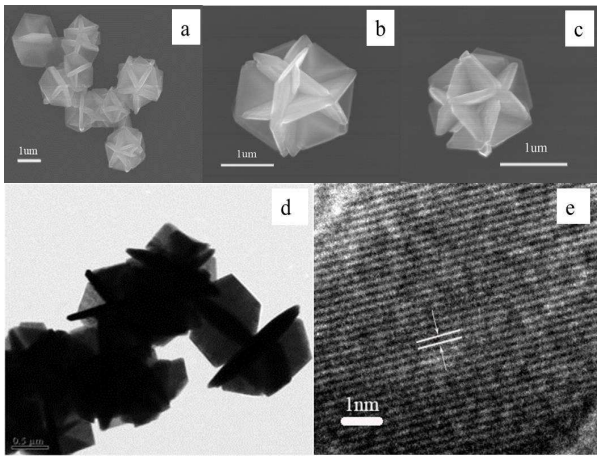

Fig. 1 Characterization of CuS caved superstructures morphology: (a) SEM, (b) and (c) magnified SEM, (d) TEM, (e) HRTEM images

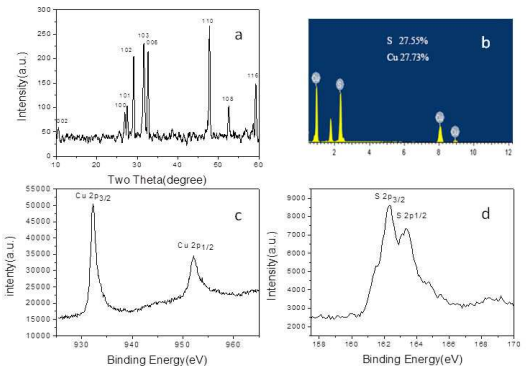

Fig. 2 Composition and structural characterizations of CuS caved superstructures by: (a) XRD, (b) EDS, (c) and (d) XPS.

To verify that our 3-D CuS caved superstructures had larger specific surface area, the Brunauer Emmett Teller (BET) surface areas and the pore volume of our sample were determined to be 13.6 m^2g^{-1} and 0.016 cm^3g^{-1}. The nitrogen adsorption-desorption isotherms of our CuS materials show representative type Ⅱ curves, indicating the presence of porous structures (Fig. S1a†). The pore size distribution curves of our materials indicate a wide distribution from 1 to 14 nm, further confirming the existence of porous structures (Fig. S1b†). Because the large specific surface area can provide more surface active sites for the adsorption of reactant molecules, the heterogeneous catalytic processes become more efficient with greater specific surface area.[56, 58-60] Therefore, the 3-D structure of our CuS caved superstructures should improve their catalytic activity because of the large specific surface area they exhibit.

3.2 Size and morphology control of CuS products.

Using our synthetic method, CuS caved superstructures of different sizes and morphologies could be synthesized by adjusting the reaction conditions. SEM images of CuS products synthesized at reaction temperatures of 110 ^oC, 120 ^oC, 130 ^oC and 140 ^oC, Supporting formation (Fig. S2†), indicate that the CuS products have regular morphology and uniform size. We find that there are few hexagonal flakes formed at these reaction temperatures. The CuS products were especially uniform size and morphology at 120 ^oC.

Supporting formation (Fig. S3†) displays SEM images of CuS caved superstructures obtained at 150 ^oC, 160 ^oC and 170 ^oC. The morphology of the CuS caved superstructures is similar, and their diameters, ranging from 800 nm to 2μm, decreased as the temperature of the dissolved $CuSO_4$ increased from 150 ^oC to 160 ^oC, 170 ^oC. This might be due to the faster rate of diffusion and nucleation at high temperature. Thus, the temperature of the dissolved $CuSO_4$ can play a key role in the size and morphology of CuS caved superstructures.

The temperature of the preheated EG can also be a crucial factor in the morphology of CuS materials. Without preheating the EG, our CuS materials were dispersive and contained uniform flakes (Fig. S4a†). However when EG was preheated, regular CuS caved superstructures were synthesized (Fig. S4b†). That may be because the aldehyde reductant is produced in the process of preheating EG. Thus, the amount of aldehyde produced in preheating influences the rate of nucleation, which then influences the morphology of CuS materials.

Using this observation, we proposed that the precursor ratios affected the morphology of products. To test this, three different molar ratios of Cu_2SO_4 and sulphur powder were used in our synthesis. Supporting formation (Fig. S5†) shows the size and morphology of products synthesized with Cu_2SO_4 and sulphur powder using these molar ratios of 4:1, 2:2, 1:1 and 0.5:1. With a 1:1 Cu_2SO_4 to sulphur powder molar ratio, we observed CuS caved superstructures with regular morphologies and uniform sizes (Fig. S5c†). Notably, the products synthesized with the Cu_2SO_4 and sulphur powder molar ratios of 4:1and 0.5:1 were almost entirely made of flakes (Fig. S5a† and S5d†). These results show that the precursor ratios play a clear role in the morphology of the CuS caved superstructures

3.3 Mechanism of formation and growth for CuS caved superstructures.

We found that the amount of EG in the system is important for forming a stable CuS spherical morphology. This is because EG is the only reducing agent in the reaction system, producing acetaldehyde as a reductant. According to Fievet et al. [61] and Wu et al.,[62] the reaction could proceed in this fashion:

$$HOCH_2CH_2OH \rightarrow CH_3CHO+H_2O \quad (1)$$

$$2CH_3CHO + S \rightarrow CH_3COCOCH_3+2H_2S \quad (2)$$

$$Cu^{2+}+ H_2S \rightarrow CuS+2H^+ \quad (3)$$

In this mechanism, acetaldehyde is produced as an important reducing agent from EG (Equation 1). H_2S molecules, which combine with Cu^{2+} and produce CuS nuclei rapidly (Equation 3), are formed through the reduction of S atoms by acetaldehyde (Equation 2). The strong affinity of Cu^{2+} and S^{2+}, and the insolubility of CuS in EG drive the reaction in the forward direction.

To identify the growth mechanism of CuS caved superstructures, we monitored the morphology by intercepting intermediate products at different time intervals using the time-dependent SEM observations. As shown in Fig. 3, the change in shape and size of the products is greatly dependent on the reaction time. We observed a continuous morphological evolution from nanospheres with rough surfaces to microspheres with regular and beautiful shapes. During the time these structures were observed, the nanospheres had almost invariable size and the rough surface diminished and thickened within 2 min (Fig. 3a-c). After this time, irregular nanoplates disappeared and transformed into nanodisks (Fig. 3d). At 6 min, the nanospheres turned into microspheres and nanodisks also became microdisks (Fig. 3e-f). Further extension of the reaction time to 10 min formed regular nanospheres with a size of approximately 2 μm made up of several intersecting hexagonal microplates (Fig. 3h-i).

We propose a growth pattern mechanism to explain formation of the CuS caved superstructures (Scheme 1). Similar to the impact of the CTAB surfactant on Cu_2Se nuclei growth,[63] the PVP used in our synthesis plays a key role in crystal growth of CuS caved superstructures. Initially, few CuS crystal nuclei with surfaces that can be effectively covered are formed.[63] With longer reaction times, CuS nanoparticles tend to assemble into nanospheres that exhibit rough surfaces, decreasing the nanoparticle surface energy. The rough surface provides many high-energy sites for oriented nanocrystal growth. During the initial stage of CuS nanosphere growth, nanosphere flakes gradually dissolve along low-energy sites and recrystallize along high-energy sites. In this fashion, the formation of regular CuS caved superstructures could get through the mass diffusion and Ostwald ripening process[31]. The formation of regular CuS plates may be attributed to the preferential growth direction along the (110) plane and the stacking faults planes.[64] As a result, different morphology and size of CuS particles can be readily synthesized by controlling the appropriate reaction conditions, as shown previously.[33]

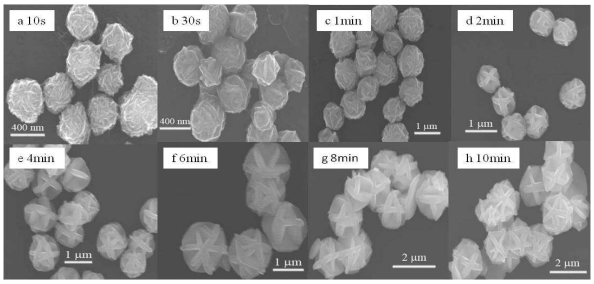

Fig. 3 The SEM images of CuS caved superstructures. a-i) SEM images of CuS caved superstructures showed the shape evolution of intermediates at reaction time. $CuSO_4$ dissolved temperature was 160 °C in the EG

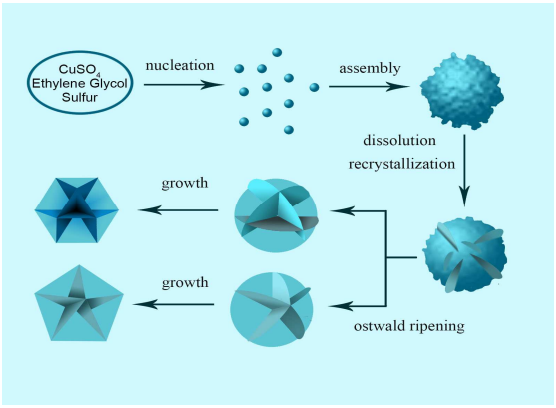

Scheme 1. Schematic illustration of a possible CuS caved superstructures growth mechanism

3.4 Catalytic activity of CuS caved superstructures

To investigate their catalytic properties, our CuS products were used to catalyze MB degradation in the presence of H_2O_2 in visible light. As shown in Fig. 4, the catalytic activity of our synthetic CuS materials was measured using UV-Vis absorption. First, we studied how the quantity of H_2O_2 and CuS caved superstructures impacted MB degradation (Fig. 4a and 4b). Fig. 4a shows that 300μl H_2O_2 has a suitable impact on the rate of MB degradation. It was found that the MB degradation rate gradually increased as the quantity of CuS increased from 2.5 to 10 mg in the presence of 300μl H_2O_2 (Fig. 4b). Fig. 4c and 4d showed the UV-Vis absorption spectra of a MB solution with hexagonal nano/microflakes and CuS caved superstructures at different time intervals in visible light. The obvious decrease in absorption indicates that the degradation of MB has occurred with the addition of the our CuS caved superstructures (Fig. 4d). Fig. 4f showed the MB degradation dynamics of different reactions, which could be expressed by plotting $(c_0-c_t)/c_0$ as a function of time. As shown in Fig. 4e (curves 1 and 2), the catalytic reaction was very slow when only H_2O_2 or CuS are present in solution and could be greatly accelerated with the addition of CuS caved superstructures. With this addition, 95% of MB was degradated within 5 min (curve 3 in Fig. 4e). This was an improvement over the weak degradation observed with the addition of CuS nano/microflakes (curve 5 in Fig. 4e). The possible reason was that the nano/microspheres possessed larger specific surface area than that of nano/microflakes. It is important to note that the ratio of MB degradation by the CuS caved superstructure catalyst was almost equivalent in visible light and in the dark (curves 3 and 4 in Fig. 4e). This is in contrast with previous reports where light was required for MB degradation.[28-32, 34] We also investigated the reusability of our CuS caved superstructure catalyst.

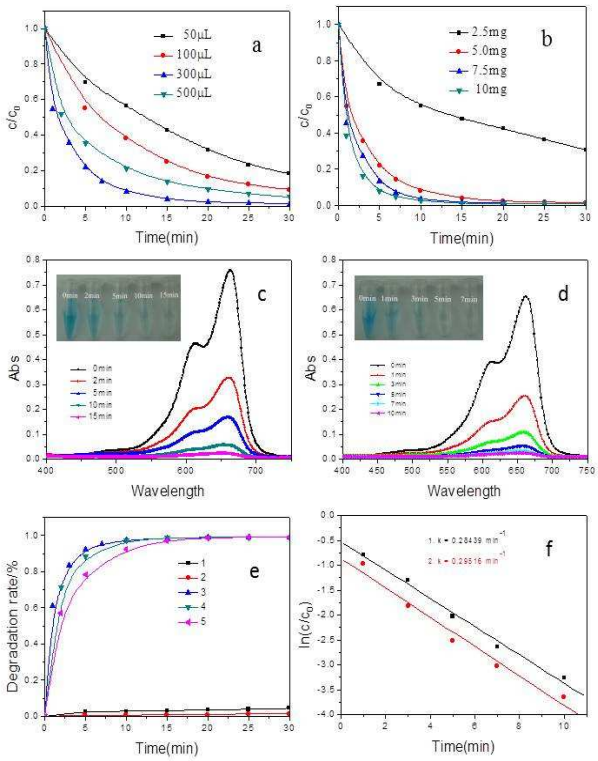

Fig.4 (a) and (b) Plot of c/c_0 vs time (T) with different H_2O_2 volumes and quantity of CuS caved superstructures. (c) UV−Vis absorption spectra of MB dye upon adding CuS nano/microflakes and H_2O_2, the inset image indicates the decoloration reaction. (d) UV−Vis absorption spectra of MB in the presence of CuS caved superstructures and H_2O_2, the inset image indicates the decoloration reaction. (e) The MB degradation rate in the presence of (1) H_2O_2 in visible light, (2) CuS caved superstructures in visible light, (3) H_2O_2 and CuS caved superstructures in visible light, (4) H_2O_2 and CuS caved superstructures in the dark, (5) H_2O_2 and CuS nano/microflakes in visible light. (f) Plot of $\ln(c/c_0)$ vs time (T) with CuS (1. 7.5 mg, 2. 10 mg).

The degradation ratio of MB for the first cycle was 96.6% (Fig. S6a†). The catalytic performance was found to maintain a 91% ratio after five cycles. SEM image showed that the morphology of the CuS caved superstructures remained unchanged after five reaction cycles, in comparison to their morphology prior to the reaction. This indicates that the our CuS caved superstructures are very stable, making this type of material a potential candidate for a recyclable Fenton-like reagent (Fig. S6b).[30, 65]

3-D CuS with hierarchical structures have been shown to be high-efficiency Fenton-like reagents.[30, 65] Basu et al. verified that OH• radicals react with organic dyes to oxidize and eventually mineralize them.[52] The catalytic activity of the 3-D CuS completely degraded the MB within 10 min (Fig 4d). We ascribed this to the yield of a hydroxide radical in the following reaction mechanism, where RH represents organic substrates such as MB.[30, 66]

$$Cu^{2+} + H_2O_2 \rightarrow H^+ + CuOOH^+ \quad (4)$$
$$CuOOH^+ \rightarrow HOO\bullet + Cu^+ \quad (5)$$
$$2HOO\bullet \rightarrow 2OH\bullet + O_2 \quad (6)$$
$$Cu^+ + H_2O_2 \rightarrow Cu^{2+} + OH\bullet + OH^- \quad (7)$$
$$RH + HO\bullet \rightarrow R\bullet + H_2O \quad (8)$$
$$R\bullet + O_2 \rightarrow \text{degraded or mineralized products} \quad (9)$$

To verify that OH• was generated from the decomposition of H_2O_2 in the presence of a CuS catalyst, electron spin resonance (ESR) was used to detect oxygen-related radicals due to their short lifetime. 5,5-dimethyl-1-pyrroline-*N*-oxide (DMPO) was used as a specific target to capture OH• in the detection process of OH•. Fig. 5 shows the

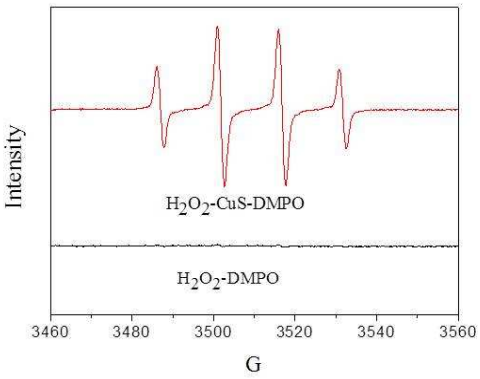

Fig. 5 DMPO−OH· adduct in the presence (red line) or absence (blackline) of CuS caved superstructures. Conditions: modulation amplitude, 1.944 G; microwave power, 1.002e + 001 mW; receiver gain, 1.00e + 005; sweep width, 100.00 G. The ESR measurements were achieved with a Bruker ESP-300E spectrometer operating in the X-band at room temperature.

signal intensity enhancement of the ESR spectra in the presence of CuS caved superstructures and strongly suggests that a high amount of OH• was generated in the catalytic reaction. From this we see that our CuS caved superstructures act catalytically to accelerate the decomposition of H_2O_2 and generate a high yield of OH• on their surface.

The dynamic features of the catalytic activity of the our CuS can be further derived from Fig 4b, resulting in a straight plot of ln$A$ versus T with negative slope (Fig. 4f). The linearity of the plot suggests that the catalytic decomposition reaction of MB by CuS caved superstructures obeys pseudo-first order kinetics, as expressed by the equation, wherein A and A_0 are the absorbance at time t and t_0, while k is the reaction rate constant.

$$\ln \frac{A}{A_0} = -kt$$

It is well-known that a higher k value indicates a faster reaction rate. These results indicate that CuS caved superstructures are very effective catalysts for MB decomposition.

Conclusions

3-D CuS caved superstructures and CuS hexagonal nano/microflakes have been synthesized by a simple, template-free solvothermal process at moderate temperature (120 ^oC), under normal pressure. This study provides a convenient, economical, and large-scale method for preparing a CuS catalyst with controllable size, structure, and morphology. A possible growth pattern has been proposed to explain the formation of CuS caved superstructures by analyzing the time-dependent SEM images of CuS particles. Our 3-D CuS caved superstructures exhibit high catalytic activity in the degradation of MB, which was verified through kinetic analysis. Because of their low cost, easy preparation, and highly efficient catalytic activity, metal chalcogenide nano/microstructures represent promising candidates for the treatment of dye contaminated waste water.

Acknowledgements

This work was partially supported by the National Natural Science Foundation of China (NSFC, No. 21375109). Also, this work was financially supported by the Fundamental Research Funds for the Central Universities of China (No. XDJK2013C036)

Notes and references

[a]*Key Laboratory of Luminescent and Real-Time Analytical Chemistry (Southwest University), Ministry of Education, College of Chemistry and Chemical Engineering, Southwest University, Chongqing 400715. E-mail: chengzhi@swu.edu.cn; Fax/Tel: (+86)-23-68254659.*

[b]*College of Pharmaceutical Sciences, Southwest University, Chongqing 400715, PR China.*

[c]*College of Chemical Engineering, Guizhou University of Engineering Science, Guizhou 551700.*

† Electronic Supplementary Information (ESI) available. See DOI: 10.1039/a000000x/

1. Y. Zhao, H. Pan, Y. Lou, X. Qiu, J. Zhu, C. Burda, *J Am Chem Soc.*, 2009, **131**, 4253–4261.
2. S. Q. Lie, D. M. Wang, M. X. Gao and C. Z. Huang, *Nanoscale*, 2014, **6**, 10289-10296.
3. S. Q. Lie, H. Y. Zou, Y. Chang and C. Z. Huang, *RSC Adv.*, 2014, **4**, 55094-55099.
4. W. L. Li, S. Q. Lie, Y. Q. Du, X. Y. Wan, T. T. Wang, J. Wang and C. Z. Huang, *J. Mater. Chem. B*, 2014, **2**, 7027-7033.
5. J. S. Chung and H. J. Sohn, *J. Power Sources*, 2002, **108**, 226-231.
6. Y. Chen, C. Davoisne, J.-M. Tarascon and C. Guery, *J. Mater. Chem.* , 2012, **22**, 5295-5299.
7. R. S. Mane and C. D. Lokhande, *Mater. Chem. Phys.*, 2000, **65**, 1-31.
8. Y. Wu, C. Wadia, W. Ma, B. Sadtler and A. P. Alivisatos, *Nano Lett.*, 2008, **8**, 2551-2555.
9. T. Sakamoto, H. Sunamura, H. Kawaura, T. Hasegawa, T. Nakayama and M. Aono, *Appl. Phys. Lett.*, 2003, **82**, 3032-3034.
10. X. Zhang, G. Wang, A. Gu, Y. Wei and B. Fang, *Chem. Commun.*, 2008, 5945-5947.
11. J. Liu and D. Xue, *J. Mater. Chem.*, 2011, **21**, 223-228.
12. S. Zhang, H. Zhong and C. Ding, *Anal. Chem.*, 2008, **80**, 7206-7212.
13. J. Bai and X. Jiang, *Anal. Chem.*, 2013, **85**, 8095-8101.
14. A. K. Dutta, S. Das, S. Samanta, P. K. Samanta, B. Adhikary and P. Biswas, *Talanta*, 2013, **107**, 361-367.
15. Y.-D. Zhu, J. Peng, L.-P. Jiang and J.-J. Zhu, *Analyst*, 2014, **139**, 649-655.
16. C. Ding, H. Zhong and S. Zhang, *Biosens. Bioelectron.*, 2008, **23**, 1314-1318.
17. M. Zhou, R. Zhang, M. Huang, W. Lu, S. Song, M. P. Melancon, M. Tian, D. Liang and C. Li, *J. Am. Chem. Soc.*, 2010, **132**, 15351-15358.
18. Z. Zha, S. Wang, S. Zhang, E. Qu, H. Ke, J. Wang and Z. Dai, *Nanoscale*, 2013, **5**, 3216-3219.
19. Y. Wang, Y. Xiao, H. Zhou, W. Chen and R. Tang, *RSC Adv.*, 2013, **3**, 23133-23138.
20. K. Dong, Z. Liu, Z. Li, J. Ren and X. Qu, *Adv. Mater.*, 2013, **25**, 4452-4458.
21. Z. Zha, S. Zhang, Z. Deng, Y. Li, C. Li and Z. Dai, *Chem. Commun.*, 2013, **49**, 3455-3457.
22. G. Ku, M. Zhou, S. Song, Q. Huang, J. Hazle and C. Li, *ACS Nano*, 2012, **6**, 7489-7496.
23. T. Zhu, B. Xia, L. Zhou and X. Wen Lou, *J. Mater. Chem.*, 2012, **22**, 7851-7855.
24. H. Peng, G. Ma, K. Sun, J. Mu, H. Wang and Z. Lei, *J. Mater. Chem. A*, 2014, **2**, 3303-3307.
25. S. Ramadan, L. Guo, Y. Li, B. Yan and W. Lu, *Small*, 2012, **8**, 3143-3150.
26. M. Nagarathinam, K. Saravanan, W. L. Leong, P. Balaya and J. J. Vittal, *Cryst. Growth Des.*, 2009, **9**, 4461-4470.
27. A. M. Malyarevich, N. N. Posnov, K. V. Yumashev, V. S. Gurin, A. A. Alekseenko, V. B. Prokopenko and I. M. Mel'nichenko, *J. Appl. Spectrosc.*, 2000, **67**, 699-704.
28. T.-Y. Ding, M.-S. Wang, S.-P. Guo, G.-C. Guo and J.-S. Huang, *Mater. Lett.*, 2008, **62**, 4529-4531.
29. F. Li, J. Wu, Q. Qin, Z. Li and X. Huang, *Powder Technol.*, 2010, **198**, 267-274.
30. Z. Li, L. Mi, W. Chen, H. Hou, C. Liu, H. Wang, Z. Zheng and C. Shen, *CrystEngComm*, 2012, **14**, 3965-3971.
31. X. Meng, G. Tian, Y. Chen, R. Zhai, J. Zhou, Y. Shi, X. Cao, W. Zhou and H. Fu, *CrystEngComm*, 2013, **15**, 5144-5149.

32. L. Mi, W. Wei, Z. Zheng, Y. Gao, Y. Liu, W. Chen and X. Guan, *Nanoscale*, 2013.
33. W. He, H. Jia, X. Li, Y. Lei, J. Li, H. Zhao, L. Mi, L. Zhang and Z. Zheng, *Nanoscale*, 2012, **4**, 3501-3506.
34. M. Wang, F. Xie, W. Li, M. Chen and Y. Zhao, *J. Mater. Chem. A*, 2013, **1**, 8616-8621.
35. J. Kundu and D. Pradhan, *ACS Appl. Mater. Inter.*, 2014, **6**, 1823-1834.
36. H. Zhu, J. Wang and D. Wu, *Inorg. Chem.*, 2009, **48**, 7099-7104.
37. M. Nagarathinam, J. Chen and J. J. Vittal, *Cryst. Growth Des.*, 2009, **9**, 2457-2463.
38. L. Ge, X.-y. Jing, J. Wang, S. Jamil, Q. Liu, D.-l. Song, J. Wang, Y. Xie, P.-p. Yang and M.-l. Zhang, *Cryst. Growth Des.*, 2010, **10**, 1688-1692.
39. Z.-h. Yang, D.-p. Zhang, W.-x. Zhang and M. Chen, *J. Phys. Chem. Solids*, 2009, **70**, 840-846.
40. J. Gao, Q. Li, H. Zhao, L. Li, C. Liu, Q. Gong and L. Qi, *Chem. Mater.*, 2008, **20**, 6263-6269.
41. S. Wan, F. Guo, L. Shi, Y. Peng, X. Liu, Y. Zhang and Y. Qian, *J. Mater. Chem.*, 2004, **14**, 2489-2491.
42. C. Deng, X. Ge, H. Hu, L. Yao, C. Han and D. Zhao, *CrystEngComm*, 2014, **16**, 2738-2745.
43. P. Leidinger, R. Popescu, D. Gerthsen, H. Lunsdorf and C. Feldmann, *Nanoscale*, 2011, **3**, 2544-2551.
44. S. Jiao, K. Jiang, Y. Zhang, M. Xiao, L. Xu and D. Xu, *J. Phys. Chem. C*, 2008, **112**, 3358-3361.
45. S. Sun, X. Song, C. Kong, S. Liang, B. Ding and Z. Yang, *CrystEngComm*, 2011, **13**, 6200-6205.
46. S. Sun, X. Song, C. Kong, D. Deng and Z. Yang, *CrystEngComm*, 2012, **14**, 67-70.
47. Z. Cheng, S. Wang, Q. Wang and B. Geng, *CrystEngComm*, 2010, **12**, 144-149.
48. X.-H. Guan, P. Qu, X. Guan and G.-S. Wang, *RSC Adv.*, 2014, **4**, 15579-15585.
49. S. Gorai, D. Ganguli and S. Chaudhuri, *Cryst. Growth Des.*, 2005, **5**, 875-877.
50. M. Tanveer, C. Cao, Z. Ali, I. Aslam, F. Idrees, W. S. Khan, F. K. But, M. Tahir and N. Mahmood, *CrystEngComm*, 2014, **16**, 5290-5300.
51. X. L. Yu, C. B. Cao, H. S. Zhu, Q. S. Li, C. L. Liu and Q. H. Gong, *Adv. Funct. Mater.*, 2007, **17**, 1397-1401.
52. M. Basu, A. K. Sinha, M. Pradhan, S. Sarkar, Y. Negishi, Govind and T. Pal, *Environ. Sci. Technol.*, 2010, **44**, 6313-6318.
53. T. Kuzuya, K. Itoh, M. Ichidate, T. Wakamatsu, Y. Fukunaka and K. Sumiyama, *Electrochim. Acta*, 2007, **53**, 213-217.
54. J. Yu, J. Zhang and S. Liu, *J. Phys. Chem. C*, 2010, **114**, 13642-13649.
55. C.-K. Wu, M. Yin, S. O'Brien and J. T. Koberstein, *Chem. Mater.*, 2006, **18**, 6054-6058.
56. J. Zhang, J. Yu, Y. Zhang, Q. Li and J. R. Gong, *Nano Lett.*, 2011, **11**, 4774-4779.
57. J. Ghijsen, L. H. Tjeng, J. van Elp, H. Eskes, J. Westerink, G. A. Sawatzky and M. T. Czyzyk, *Phys. Rev. B*, 1988, **38**, 11322--11330.
58. M. R. Hoffmann, S. T. Martin, W. Choi and D. W. Bahnemann, *Chem. Rev.*, 1995, **95**, 69-96.
59. J. Yu, L. Zhang, B. Cheng and Y. Su, *J. Phys. Chem. C*, 2007, **111**, 10582-10589.
60. J. Yu, W. Wang and B. Cheng, *Chem. Asian J.*, 2010, **5**, 2499-2506.
61. F. Fievet, J. P. Lagier, B. Blin, B. Beaudoin and M. Figlarz, *Solid State Ionics*, 1989, **32–33, Part 1**, 198-205.
62. C. Wu, S.-H. Yu and M. Antonietti, *Chem. Mater.*, 2006, **18**, 3599-3601.
63. J. Zhu, Q. Li, L. Bai, Y. Sun, M. Zhou and Y. Xie, *Chem–Eur. J.*, 2012, **18**, 13213-13221.
64. A. Ghezelbash and B. A. Korgel, *Langmuir*, 2005, **21**, 9451-9456.
65. L. Mi, W. Wei, Z. Zheng, G. Zhu, H. Hou, W. Chen and X. Guan, *Nanoscale*, 2014, **6**, 1124-1133.
66. T. Rhadfi, J.-Y. Piquemal, L. Sicard, F. Herbst, E. Briot, M. Benedetti and A. Atlamsani, *Appl. Catal. A-Gen.*, 2010, **386**, 132-139.

